The Dynamics of Drops and Attached Interfaces for the Constrained Allen-Cahn Equation

Doug Stafford, Michael J. Ward, Brian Wetton[1]

Department of Mathematics
University of British Columbia
Vancouver, Canada

Abstract

The motion of interfaces for a mass-conserving Allen-Cahn equation that are attached to the boundary of a two-dimensional domain is studied. In the limit of thin interfaces, the interface motion for this problem is known to be governed by an area-preserving mean curvature flow. A numerical front-tracking method, that allows for a numerical solution of this type of curvature flow, is used to compute the motion of interfaces that are attached orthogonally to the boundary. Results obtained from these computations are favorably compared with a previously derived asymptotic result for the motion of attached interfaces that enclose a small area. The area-preserving mean curvature flow predicts that a semi-circular interface is stationary when it is attached to a flat segment of the boundary. For this case, the interface motion is shown to be metastable and an explicit characterization of the metastability is given.

1 Introduction

A simple model for the phase separation of a binary mixture is the Allen-Cahn equation with a mass constraint as introduced in [15],

$$u_t = \epsilon^2 \Delta u + Q(u) - \sigma\,, \qquad \mathbf{x} \in D \subset \mathbf{R}^2\,, \tag{1.1a}$$

$$\partial_n u = 0\,, \qquad \mathbf{x} \in \partial D\,, \tag{1.1b}$$

$$\int_D u(\mathbf{x},t)\,d\mathbf{x} = m\,. \tag{1.1c}$$

Here $u = u(\mathbf{x},t)$ is the concentration of one of the two species, $\mathbf{x} = (x,y)$, $\epsilon \ll 1$, D is a bounded two-dimensional domain, and the mass m is constant. We assume that $Q(u) = -V'(u)$, where $V(u)$ is a double-well potential with minima at $u = s_\pm$ where $V(s_\pm) = 0$. The function $Q(u)$ satisfies

$$Q(s_\pm) < 0\,, \quad Q(0) > 0\,, \quad V(s_+) = 0\,, \quad V(u) = -\int_{s_-}^{u} Q(\eta)\,d\eta\,. \tag{1.2}$$

Prototypical is $Q(u) = u - u^3$. The Lagrange multiplier parameter $\sigma = \sigma(t)$ allows the mass constraint (1.1c) to be satisfied. A generic feature of the nonlocal problem (1.1) in the singularly perturbed limit $\epsilon \to 0$ is the occurrence of interfaces of width $O(\epsilon)$ that separate the two phases s_+ and s_-.

[1]All three authors supported by Canadian NSERC research grants

In the limit $\epsilon \to 0$, our goal is to study the motion of interfaces for (1.1) that are attached to the boundary of D. Before describing the specific contents of this paper, we outline the different stages of the dynamics for (1.1) that have been studied in detail in [1], [2], [3], [4], [15] and [16]. The various stages of the dynamics of a single closed interface for (1.1) are shown qualitatively in Fig. 1.

The first stage is a transient phase. Starting from arbitrary initial data, the solution to (1.1) develops interfaces of width $O(\epsilon)$ separating s_+ and s_- in an $O(1)$ time interval. Then, as derived in [15] in the limit $\epsilon \to 0$, the outward normal velocity v of a single closed interface Γ satisfies the area-preserving mean curvature flow

$$v \sim \epsilon^2 \left(\kappa - \frac{1}{|\Gamma|} \int_\Gamma \kappa \, ds \right) . \tag{1.3}$$

Here κ is the curvature of Γ, with $\kappa < 0$ if Γ is a circle, and $|\Gamma|$ is the perimeter of Γ. This expression holds for interfaces in the interior of D and for interfaces that are connected to ∂D orthogonally. As shown in [9], a single closed convex interface evolving according to (1.3) will tend to a circle that encloses the same area.

The law of motion (1.3) gives no indication of the nature of the motion of a single circular interface contained in D. Such an interface, referred to as a *bubble*, was shown in [3], [4], and [16] to drift exponentially slowly, without change of shape, towards the closest point on ∂D. The key features that lead to this metastable behavior are the conservation of mass condition combined with the exponentially weak interaction between the far-field behavior of the bubble solution and the boundary ∂D. It was derived in [16] that the distance $r_m(t)$ between the center of the bubble and the closest point on the boundary of D, satisfies the asymptotic differential equation

$$r_m'(t) \sim - \frac{\epsilon^{3/2} \zeta r_m^{-1/2}}{(1 - \mathcal{K}_m r_m)^{1/2}} e^{-2\nu_+^\epsilon \epsilon^{-1}(r_m - r_b)} . \tag{1.4}$$

Here $\mathcal{K}_m$ is the curvature of ∂D at the point on ∂D closest to the bubble center, with $\mathcal{K}_m > 0$ when D is convex at the closest point. In addition, r_b is the bubble radius, and ν_+^ϵ and ζ are certain $O(1)$ positive constants. This result, which is asymptotically valid only when $r_m(t) > r_b$, shows that the bubble will collapse against ∂D on an exponentially long time scale.

Once the bubble hits ∂D, it presumably becomes quickly attached to ∂D orthogonally and its boundary becomes the arc of a circle in order to minimize its perimeter. Its subsequent evolution is then given by (1.3). However, if the length scale of the interface is sufficiently small compared to the radius of curvature of ∂D, the interface will become approximately semi-circular in shape. The motion of such a semi-circular *drop* of radius δ, with $\delta \ll 1$, has been studied in [2]. It was shown in [2] that the center of a such a small drop of radius δ, with $\delta \ll 1$ but $0 < \epsilon < \delta^3$, satisfies the asymptotic ODE

$$\xi'(t) \sim \frac{4\epsilon^2 \delta}{3\pi} \mathcal{K}'(\xi(t)) . \tag{1.5}$$

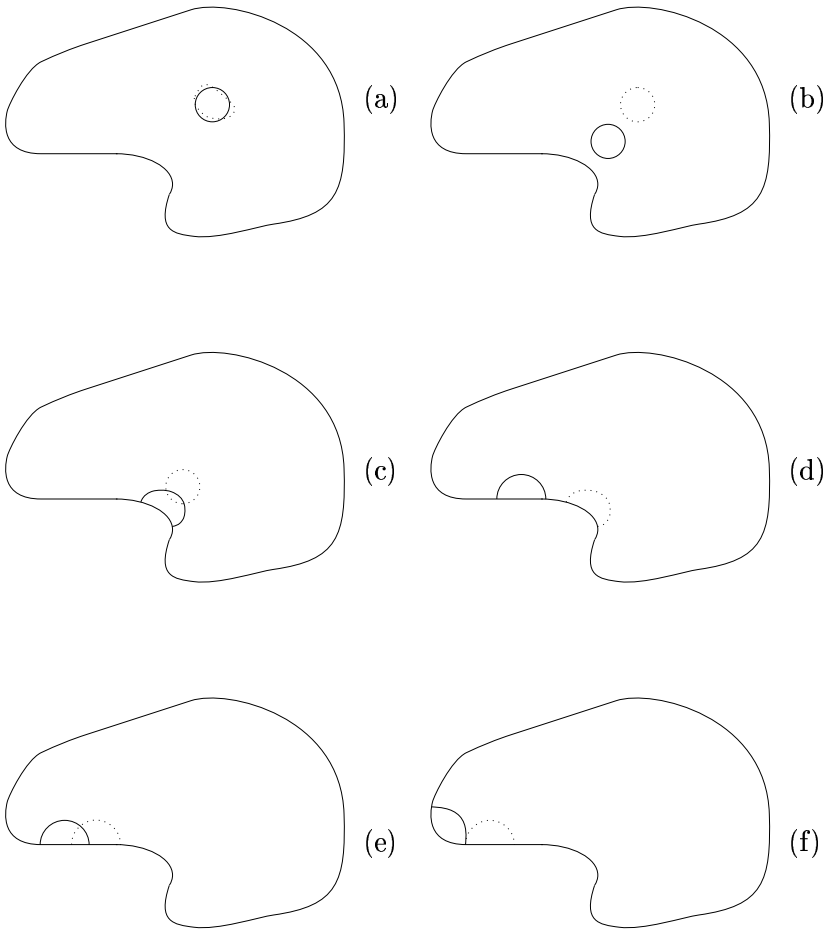

Figure 1: Evolution of a small convex interface inside a domain D. (a) The convex interface evolves by (1.3) into a circle. (b) The bubble drifts, satisfying (1.4), towards the closest point on ∂D. (c) The interface attaches to ∂D, intersecting orthogonally. (d) The interface moves along ∂D satisfying (1.3), or (1.5) when the interface encloses a small area. (e) If the interface encounters a flat portion of ∂D, it moves along this flat portion exponentially slowly according to (3.28a). (f) When a curved part of ∂D is reached, the interface again evolves by (1.3) until a steady state is attained, which is centered near a local maximum of the curvature of ∂D.

Here ξ is arclength along ∂D, δ is the radius of the drop, and $\mathcal{K}$ is the curvature of ∂D (positive for a convex domain D). The drop will reach a stable equilibrium, where the interface can have minimum perimeter, at a local maximum of $\mathcal{K}$. For interfaces enclosing a finite area, for which (1.3) applies, it was proved in [7] that there will be a local maximum of $\mathcal{K}$ between the two points on ∂D where the equilibrium interface is attached.

One goal of this paper is to determine the range of validity of the small drop result (1.5) by comparing the motion under (1.5) with the corresponding motion under the area-preserving mean curvature flow (1.3). To study the motion of attached interfaces under (1.3) we use the front-tracking method developed in [6], combining the algorithms developed there for nonlocal curvature motion and orthogonal boundary attachment and extending the code to handle more general boundary geometries. By comparing results obtained from this numerical method with those obtained from (1.5), we conclude that the asymptotic differential equation (1.5) provides rather accurate results even for drops of only a moderately small radius.

The second purpose of this paper is to study the motion of a semi-circular interface that is attached orthogonally to a flat portion of the boundary. In this case, both (1.3) and the small drop result (1.5) predict that such a semi-circular interface is stationary on the time interval $t = O(\epsilon^{-2})$. We show that the motion of a semi-circular interface on a flat portion of the boundary is metastable and depends critically on the local behavior of the boundary at the ends of the flat segment. An asymptotic differential equation for the motion of the center of the semi-circular interface on the flat boundary segment is derived.

The outline of the paper is as follows. In §2 we present a numerical front-tracking algorithm to study (1.3) when the interface is attached orthogonally to the boundary of the domain. The numerical results for the interface motion are compared with the asymptotic result (1.5) for drops of a small radius. In §3 we analyze the metastable behavior associated with the motion of a semi-circular interface on a flat portion of the boundary. Some conclusions are given in §4.

2 Numerical Motion by Curvature and Small Drop Motion

In §2.1 we outline the numerical front-tracking method of [6] to compute the motion of a collection of interfaces Γ_i, for $i = 1, \ldots, M$, that satisfy an area-preserving mean curvature flow. The outward normal velocity v_i of the i^{th} interface, Γ_i, is determined from

$$v_i \sim \epsilon^2 \left(\kappa_i - \frac{1}{|\Gamma|} \sum_{j=1}^{M} \int_{\Gamma_j} \kappa_j \, ds \right) . \tag{2.1}$$

Here κ_i is the curvature of Γ_i, with $\kappa_i < 0$ when Γ_i is convex, and $|\Gamma|$ is the total length of all the interfaces. This system was derived in [15] from an asymptotic analysis of (1.1) in the limit $\epsilon \to 0$. In §2.1 we describe the method of [6] used to compute the motion of interfaces moving with nonlocal curvature motion that are attached orthogonally to ∂D.

Some numerical results are presented in §2.2, where we compare the motion of small drops satisfying the asymptotic result (1.5) with the numerically computed area-preserving mean curvature flow (2.1).

2.1 The Numerical Method for Area-Preserving Mean Curvature

To eliminate the dependence on ϵ, we set $\tau = \epsilon^2 t$. We assume that the interfaces, Γ_i for $i = 1, \ldots, M$, are given parametrically by $\mathbf{x}^i(\sigma, \tau) = (x^i(\sigma, \tau), y^i(\sigma, \tau))$ where $\sigma \in [0, 1]$ (in the examples below we always consider a single curve $M = 1$ but the more general case is just as easy to compute). A partial differential equation that describes the motion under (2.1) is

$$\mathbf{x}^i_\tau = \frac{\mathbf{x}^i_{\sigma\sigma}}{|\mathbf{x}^i_\sigma|^2} - \frac{1}{|\Gamma|}\left(\sum_{j=1}^{M}\int_{\Gamma_j}\frac{\mathbf{x}^j_{\sigma\sigma}}{\left|\mathbf{x}^j_\sigma\right|^2}\cdot\hat{\mathbf{n}}_j\,ds\right)\hat{\mathbf{n}}_i\,. \tag{2.2}$$

Here $\hat{\mathbf{n}}_i$ is a unit normal to Γ_i. It is easily seen that the projection of (2.2) in the normal direction of a given interface agrees with (2.1). Note that (2.1) is arbitrary with respect to any velocity in the tangential direction. However, as shown in [6] the diffusion introduced in the tangential direction by (2.2) is helpful to smooth out derivative discontinuities in curves and to maintain a relatively uniform distribution of grid points.

Interfaces intersect the boundary at right angles. Thus, if the boundary ∂D is parameterized by $\mathbf{z}(\xi)$, where ξ is an arclength parameter, then this boundary condition can be written as

$$\mathbf{x}^i_\sigma(0,\tau)\cdot\mathbf{z}'(\xi^i_0(\tau)) = 0\,, \qquad \mathbf{x}^i_\sigma(1,\tau)\cdot\mathbf{z}'(\xi^i_1(\tau)) = 0\,. \tag{2.3a}$$

Here

$$\mathbf{x}^i(0,\tau) = \mathbf{z}(\xi^i_0(\tau))\,, \qquad \mathbf{x}^i(1,\tau) = \mathbf{z}(\xi^i_1(\tau))\,, \tag{2.3b}$$

for some $\xi^i_0(\tau)$ and $\xi^i_1(\tau)$.

The discretization procedure described here is as in [6]. We apply the method of lines, discretizing in space. A staggered grid in σ and second order centered approximations are used. We let $\mathbf{X}^i_j(\tau)$ approximate $\mathbf{x}^i((j-1/2)h, \tau)$ for $j = 0, 1, \ldots, N, N+1$, where h is the grid spacing and $N = 1/h$ is the number of interior grid points. Then to second order we have

$$\mathbf{x}^i(jh) \approx (\mathbf{X}^i_{j+1} + \mathbf{X}^i_j)/2\,. \tag{2.4}$$

The explicit dependence on time will be suppressed for the moment. Denoting the second order centered approximation of the k^{th} derivative by D_k, we have

$$\mathbf{x}^i_\sigma \approx D_1\mathbf{X}^i_j \equiv \frac{(\mathbf{X}^i_{j+1} - \mathbf{X}^i_{j-1})}{2h}\,; \qquad \mathbf{x}^i_{\sigma\sigma} \approx D_2\mathbf{X}^i_j \equiv \frac{(\mathbf{X}^i_{j+1} - 2\mathbf{X}^i_j + \mathbf{X}^i_{j-1})}{h^2}\,. \tag{2.5}$$

We estimate the normal vector, $\hat{\mathbf{n}}_i$, to an interface, Γ_i, by

$$\hat{\mathbf{n}}_i \approx \frac{(D_1\mathbf{X}_j^i)^\perp}{\left|(D_1\mathbf{X}_j^i)\right|}. \tag{2.6}$$

The integral in the second term on the right-hand side of (2.2) is approximated using these discretizations and the trapezoid rule:

$$\kappa_a \equiv \frac{1}{|\Gamma|}\sum_{i=1}^{M}\int_{\Gamma_i}\frac{\mathbf{x}_{\sigma\sigma}^i}{|\mathbf{x}_\sigma^i|^2}\cdot\hat{\mathbf{n}}_i\,ds \approx \frac{h}{|\Gamma|}\sum_{i=1}^{M}\sum_{j=1}^{N}\frac{D_2\mathbf{X}_j^i}{\left|D_1\mathbf{X}_j^i\right|^2}\cdot(D_1\mathbf{X}_j^i)^\perp. \tag{2.7}$$

The length of the interfaces is also approximated using a trapezoid scheme:

$$|\Gamma| \approx \sum_{i=1}^{M} h\sum_{j=1}^{N}\left|D_1\mathbf{X}_j^i\right|. \tag{2.8}$$

We use the approximations (2.5), (2.6), (2.7), and (2.8), to discretize (2.2) as

$$\frac{d}{d\tau}\mathbf{X}_j^i = \frac{D_2\mathbf{X}_j^i}{\left|D_1\mathbf{X}_j^i\right|^2} - \kappa_a\frac{(D_1\mathbf{X}_j^i)^\perp}{\left|D_1\mathbf{X}_j^i\right|}. \tag{2.9}$$

Here κ_a is given in (2.7). For interfaces that intersect the boundary, we apply second order forward differencing and averaging to (2.3) to obtain the following conditions:

$$(\mathbf{X}_1^i - \mathbf{z}(\xi_0^i))\cdot\mathbf{z}'(\xi_0^i) = 0, \tag{2.10a}$$

$$\mathbf{X}_0^i = 2\mathbf{z}(\xi_0^i) - \mathbf{X}_1^i, \tag{2.10b}$$

and

$$(\mathbf{X}_N^i - \mathbf{z}(\xi_1^i))\cdot\mathbf{z}'(\xi_1^i) = 0, \tag{2.11a}$$

$$\mathbf{X}_{N+1}^i = 2\mathbf{z}(\xi_1^i) - \mathbf{X}_N^i. \tag{2.11b}$$

Here $\mathbf{z}(\xi_0^i)$ and $\mathbf{z}(\xi_1^i)$ are unknown points on the boundary curve. These equations can be interpreted geometrically. From (2.10a) and (2.11a) we see that $\mathbf{z}(\xi_0^i)$ and $\mathbf{z}(\xi_1^i)$ must be the points on the boundary that are closest to $\mathbf{X}_1^i$ and $\mathbf{X}_N^i$ respectively. The points $\mathbf{X}_0^i$ and $\mathbf{X}_{N+1}^i$ are then reflections of $\mathbf{X}_1^i$ and $\mathbf{X}_N^i$ through the closest point on the boundary.

For an interface that intersects the boundary, we first use equations (2.10) and (2.11) to find $\mathbf{X}_0^i$ and $\mathbf{X}_{N+1}^i$ to ensure that the interface intersects the boundary curve orthogonally. To calculate these values for general boundaries parameterized by $\mathbf{z}(\xi)$, we first solve (2.10a) and (2.11a) numerically using the bisection method and Newton's method to determine ξ_0^i and ξ_1^i. Then, (2.10b) and (2.11b) are used to determine $\mathbf{X}_0^i$ and $\mathbf{X}_{N+1}^i$. This is done at each stage of a fourth-order Runge Kutta method and (2.9) is applied for $j = 1, 2, \ldots, N$ to advance one time step. We repeat this procedure for subsequent time steps. For stability, the time steps, k, are chosen to satisfy

$$k \le \frac{h^2}{4}\min_{i,j}\left|D_1\mathbf{X}_j^i\right|^2. \tag{2.12}$$

This time step restriction is half that needed for the stability of the frozen coefficient diffusive component of (2.9).

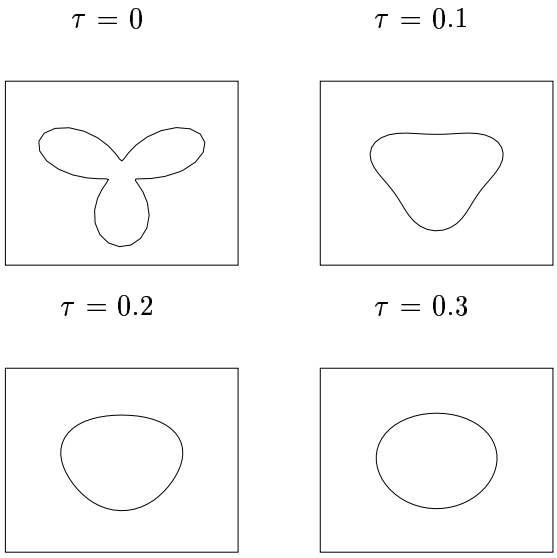

Figure 2: Evolution of a closed interface by area-preserving mean curvature.

2.2 Some Numerical Results

We now examine the evolution of interfaces in several situations using the method described in §2.1. For interfaces that enclose a small area, we compare the motion with that of (1.5).
Example 1 (Closed Interface): We now illustrate numerically the qualitative behavior seen in Fig. 1a. If the interface is initially closed and convex, then it will tend to a circle as t increases (see [9]). However, as seen in the numerical results shown in Fig. 2, certain non-convex initial interfaces can also evolve into a circle as t increases. For other initial conditions, the interface may self-intersect during its evolution and a change in the topology is needed to split the interface into more than one curve. Other situations, including the coarsening process associated with the evolution of several disjoint closed interfaces are discussed in [6].
Example 2 (Interface Attached to a Circle): In Fig. 3 we show the evolution of an interface that is attached to the unit circle. This can be viewed as a caricature of the attachment process of Fig. 1c, although the singularity structure of the initial attachment is not resolved. In this case the interface quickly evolves to an arc of a circle, and the interface does not move along the boundary. This is as expected since the evolution under (1.3) wants to minimize the length of Γ, while enclosing a specified area (see [9]).

A numerical convergence study for this example shows that the method converges pointwise with second order accuracy in the spatial discretization (errors are $O(h^2)$). In the closed curve case studied in [6], the discrete area is preserved exactly by the spatial discretization. In the current case of nonlocal curvature motion of curves attached to the boundary, this is no longer true. The discrete area is preserved up to second order accuracy, however, and in all the examples presented in this paper, area change was less than 0.1%.

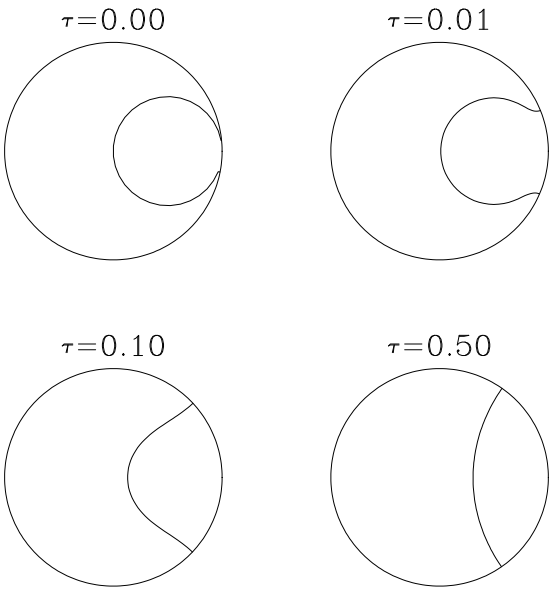

Figure 3: Evolution of an interface intersecting the unit circle.

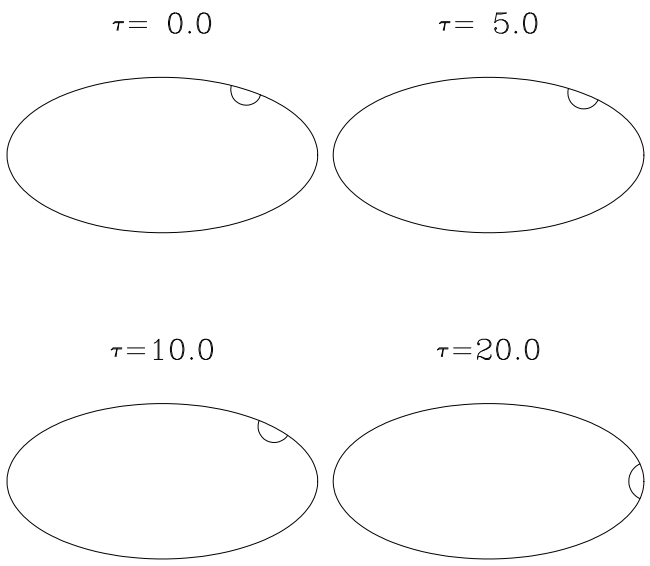

Figure 4: Evolution of an interface intersecting an ellipse. The drop shown here has radius $\delta = 0.1976$.

Example 3 (Interface Attached to an Ellipse): In Fig. 4 we show the evolution of an interface intersecting the boundary of an ellipse with semi-major axis 2 and semi-minor axis 1. In this case, ∂D can be parameterized by

$$\mathbf{z}(\theta) = (2\cos\theta, \sin\theta)\,, \quad 0 \le \theta \le 2\pi\,. \tag{2.13}$$

We observe that the interface moves along the boundary in the direction of increasing boundary curvature and it reaches a steady-state where the attachment points surround a local maximum of the boundary curvature as predicted in the steady-state analysis of [7].

Next, for the same boundary, we compared the numerical trajectories of the center of attached interfaces enclosing a small area evolving under (1.3) with the asymptotic small drop result (1.5). To do this comparison, in the numerical method of §2.1 we took the location of the center of the drop along the boundary to be the closest point on the boundary curve to the point midway between the two attachment points of the interface with the boundary. In comparing with (1.5) we need to determine the radius δ of the drop. To do so, we first calculated the area enclosed by the attached interface and the boundary using the trapezoid rule. Then, the radius δ of the drop, needed in (1.5), was estimated by assuming that the interface was semi-circular. We then track the trajectory of $\theta(\tau)$ in time as the interface evolves under the numerical method of §2.1. The results are then compared with the numerical solution of the asymptotic differential equation (1.5).

For the elliptical boundary curve defined in (2.13), the curvature of the boundary is

$\mathcal{K} = \mathcal{K}(\theta) = 2(\sin^2\theta + 4\cos^2\theta)^{-3/2}$. Thus, the asymptotic result (1.5) becomes

$$\theta'(\tau) = -\frac{24\delta}{\pi}\frac{\sin\theta\cos\theta}{(4\sin^2\theta + \cos^2\theta)^{7/2}}\,. \tag{2.14}$$

We start with the initial data of a small semi-circle centered around the point on ∂D where $\theta(0) = 1$. We observed that these drops move along the boundary in the direction of increasing boundary curvature and a steady state was reached at the local maximum of boundary curvature at $\theta = 0$. The trajectories of $\theta(\tau)$ obtained from the numerical method and the asymptotic differential equation (2.14) are compared for several different drop radii in Figure 5. As expected, we notice that the numerical trajectory gets closer to the asymptotic trajectory as δ is decreased. For very small radii, both trajectories are very similar.

Example 4 (Interface Attached to a Triangular-Shaped Domain): To generate more complicated boundary shapes, we considered boundary curves of the following form (see [11]):

$$\mathbf{z}(\theta) = (p(\theta)\cos\theta - p'(\theta)\sin\theta, p(\theta)\sin\theta + p'(\theta)\cos\theta)\,, \quad 0 \le \theta \le 2\pi\,. \tag{2.15}$$

Given any $p(\theta)$ such that $p(\theta) = p(\theta + 2\pi)$, $p(\theta) > 0$, and $p(\theta) + p''(\theta) > 0$, (2.15) generates a strictly convex domain. The curvature of such a domain is given by

$$\mathcal{K}(\theta) = \left[p(\theta) + p''(\theta)\right]^{-1}\,. \tag{2.16}$$

For this class of boundary curves, (1.5) transforms to

$$\theta'(\tau) = -\frac{4\delta}{3\pi}\frac{(p'(\theta) + p'''(\theta))}{(p(\theta) + p''(\theta))^4}\,. \tag{2.17}$$

We examined the numerical evolution of interfaces enclosing a small area for the triangular shaped domain generated by

$$p(\theta) \equiv 3 + 1.2\sin^3\theta\,. \tag{2.18}$$

This domain is plotted in Fig. 6 along with the motion of a drop along the boundary. We started with the initial data of a small semi-circle centered around the point on ∂D for which $\theta(0) = 0.2$. The location of the center of the drop, needed for the numerical prediction, and the radius of the drop, needed for (1.5), are determined as for the elliptical boundary in Example 3. Trajectories of $\theta(\tau)$ comparing the result from the numerical motion by area-preserving mean curvature with the asymptotic small drop result (2.17), are shown in Fig. 7. We observe that the motion by numerical area preserving mean curvature is very similar to the asymptotic result for small drop motion even for δ only moderately small. Thus, the numerical results in this section show that (1.5) has a rather wide range of validity and can rather accurately predict the motion of moderately small drops.

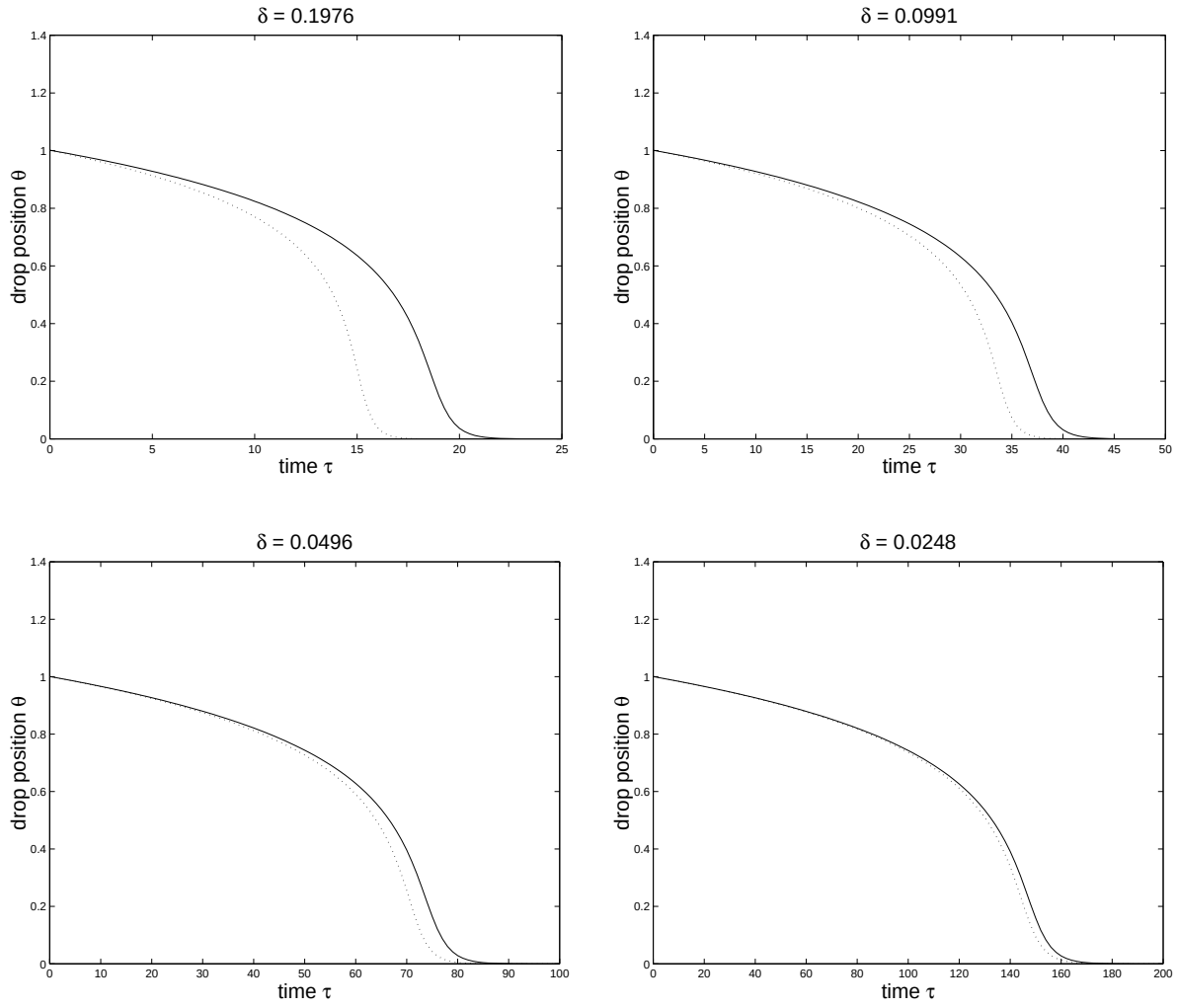

Figure 5: Plots of θ versus time for different δ. The boundary curve is the ellipse defined in (2.13). The solid lines are the asymptotic result given by (2.14) and the dashed lines are the numerical results from area-preserving mean curvature motion (1.3).

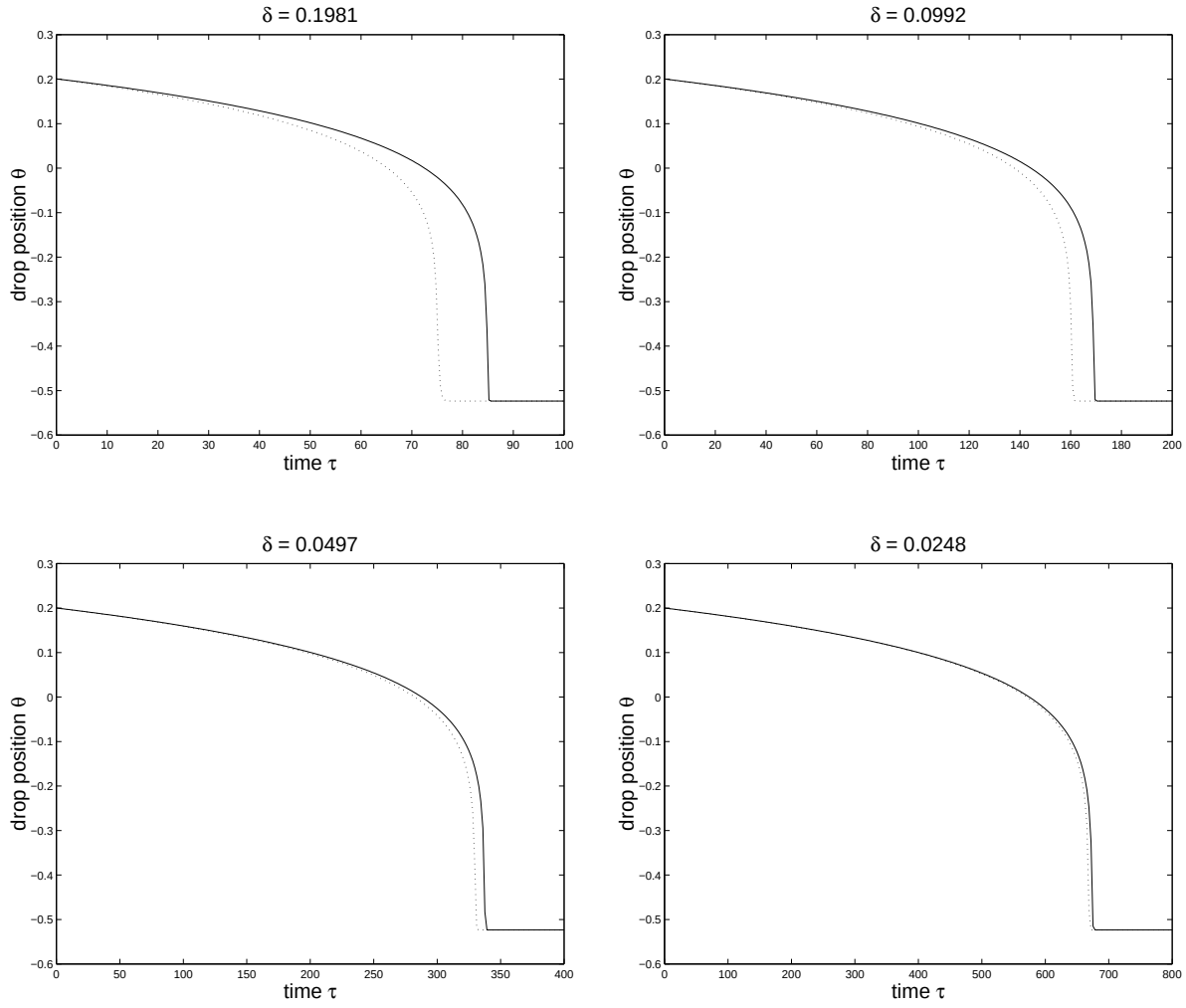

Figure 7: Plots of θ versus time for different δ. Here ∂D is parameterized by $p(\theta) \equiv 3 + 1.2\sin^3\theta$. The solid lines are the asymptotic result given by (2.17) and the dashed lines are the numerical results from area-preserving mean curvature motion (1.3).

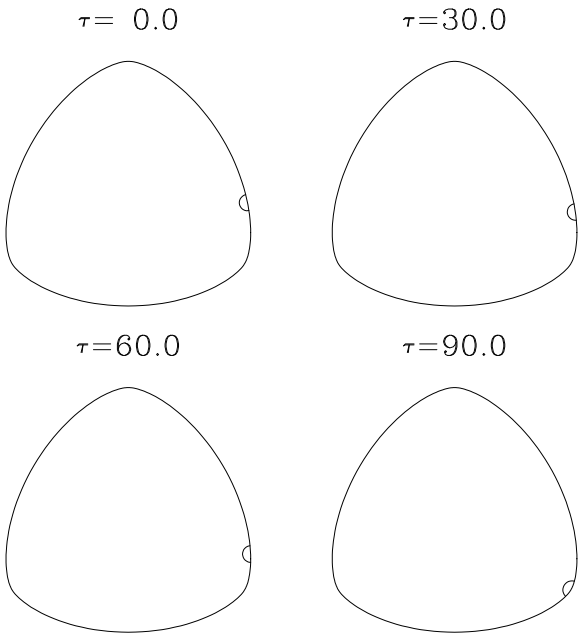

Figure 6: The domain with boundary given by $p(\theta) = 3 + 1.2\sin^3\theta$. The drop here has radius $\delta = 0.1981$.

3 The Semi-Circular Interface Motion on a Flat Boundary

We now analyze the motion of a semi-circular interface that is attached to a flat boundary. In this case, the curvature κ of the interface is constant and hence (1.3) predicts that the interface is stationary on an $O(\epsilon^{-2})$ time scale. Our analysis below shows that the interface is not stationary but, instead, moves on an exponentially long, or metastable, time scale. In §3.1 we derive an asymptotic formula for the exponentially small eigenvalue associated with the metastability. In §3.2 an asymptotic differential equation for the motion of the center $x_0(t)$ of the semi-circular interface is derived by enforcing the solvability condition that the solution to the linearized problem is orthogonal to the eigenfunction associated with the exponentially small eigenvalue. In §3.3 we discuss some properties of this differential equation and we give an explicit example.

For the analysis, we assume that the smooth boundary ∂D of D can be decomposed into a straight segment ∂D_s, occupying the region $y = 0$ with $x_L < x < x_R$, and a curved portion ∂D_c. We assume that the solution to (1.1) has developed a single semi-circular interface Γ of radius $r = r_b$ that intersects ∂D_s orthogonally. The center $\boldsymbol{x}_0 = (x_0(t), 0)$ of the semi-circle is assumed to satisfy $x_L + r_b < x_0 < x_R - r_b$. The regions near $(x_L, 0)$ and $(x_R, 0)$, where ∂D_c and ∂D_s meet, are called the corners of ∂D_s. The distance between Γ and the boundary ∂D is assumed to be a minimum at these corner points, with the minimum distance being $O(1)$ as $\epsilon \to 0$. A plot of the geometry is shown in Fig. 8.

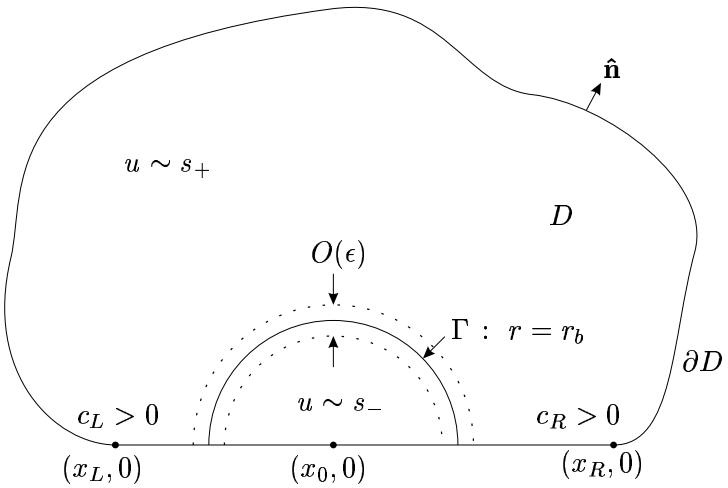

Figure 8: Plot of a two-dimensional domain D with a flat boundary segment and a semi-circular interface of radius $r = r_b$ centered at $(x_0, 0)$.

Near $(x_L, 0)$ and $(x_R, 0)$, we assume that ∂D_c can be written as $y = \psi_L(x)$ and $y = \psi_R(x)$, and that the boundary has the local behavior

$$\psi_L'(x) \sim -c_L(x_L - x)^{\alpha_L}, \quad \text{as} \quad x \to x_L^-\,; \qquad \psi_R'(x) \sim c_R(x - x_R)^{\alpha_R}, \quad \text{as} \quad x \to x_R^+\,. \tag{3.1}$$

Here $c_L \neq 0$, $c_R \neq 0$ and $\alpha_L > 0$, $\alpha_R > 0$ are constants. When $\alpha_L = \alpha_R = 1$, c_L and c_R are proportional to the curvature of ∂D_c at the left and right corner points. respectively.

We first must construct an equilibrium solution $u = U_b$, $\sigma = \sigma_b$ to (1.1) corresponding to a semi-circular interface Γ of radius r_b centered at $\boldsymbol{x}_0 = (x_0, 0) \in \partial D_s$. This solution is such that $u \sim s_-$ inside Γ and $u \sim s_+$ outside Γ. This solution was constructed asymptotically in [16] using the method of matched asymptotic expansions, and the derivation is outlined in Appendix A. It was obtained that,

$$u = U_b(r;\epsilon) \sim \begin{cases} S_+(\epsilon) - a_+(r_b/r)^{1/2} e^{-\nu_+^\epsilon \epsilon^{-1}(r - r_b)}\,, & r > r_b\,, \\ u_0(\rho) + O(\epsilon)\,, & \rho = \epsilon^{-1}(r - r_b) = O(1)\,, \\ S_-(\epsilon) + a_-(r_b/r)^{1/2} e^{-\nu_-^\epsilon \epsilon^{-1}(r_b - r)}\,, & r < r_b\,, \end{cases} \tag{3.2}$$

and

$$\sigma_b(\epsilon) = \frac{\epsilon\beta}{(s_+ - s_-)r_b} + O(\epsilon^2)\,. \tag{3.3}$$

Here $u_0(\rho)$ satisfies (A.4). The constants $S_\pm(\epsilon)$ and β are given in (A.9) and $a_\pm$, $\nu_\pm^\epsilon$ are defined in (A.5) and (A.11). In (3.2), $r = |\mathbf{x} - \mathbf{x}_0| = r_b$ and $\boldsymbol{x}_0 = (x_0, 0)$. The mass in (1.1c), which determines r_b, is assumed to be consistent with this solution.

3.1 Spectral Estimates for the Linearized Problem

The eigenvalue problem associated with linearizing (1.1) around U_b is

$$L_\epsilon \phi \equiv \epsilon^2 \Delta \phi + Q'[U_b(r;\epsilon)]\phi = \lambda \phi\,, \qquad \boldsymbol{x} \in D\,, \tag{3.4a}$$

$$\partial_n \phi = 0\,, \qquad \boldsymbol{x} \in \partial D\,, \tag{3.4b}$$

$$(\phi,\phi) = \int_D \phi^2 \, d\boldsymbol{x}\,. \tag{3.4c}$$

Here $(u,v) \equiv \int_D uv\, d\boldsymbol{x}$. The eigenvalues and eigenfunction of (3.4) are labeled by λ_j and ϕ_j, respectively for $j = 0, 1, \ldots$, with $\lambda_j \to -\infty$ as $j \to \infty$.

The principal eigenfunction and eigenvalue for (3.4) are calculated asymptotically in [16] and an outline of the analysis is given in Appendix B. The principal eigenvalue is given asymptotically by

$$\lambda_0(\epsilon) = \frac{\epsilon^2}{r_b} + O(\epsilon^3)\,, \tag{3.5}$$

and the corresponding eigenfunction has the estimate

$$\phi_0 \sim \begin{cases} R_0 a_+ \nu_+^\epsilon (r_b/r)^{1/2} e^{-\nu_+^\epsilon \epsilon^{-1}(r-r_b)}\,, & r > r_b\,, \\ R_0\left[u_0'(\rho) + O(\epsilon)\right] & \rho = \epsilon^{-1}(r-r_b) = O(1)\,, \\ R_0 a_- \nu_-^\epsilon (r_b/r)^{1/2} e^{-\nu_-^\epsilon \epsilon^{-1}(r_b-r)}\,, & r < r_b\,. \end{cases} \tag{3.6}$$

The normalization constant, R_0, satisfies

$$R_0 \sim (\epsilon \pi r_b \beta)^{-1/2}\,, \tag{3.7}$$

where β is defined in (A.9b).

In the asymptotic evaluation of the integrals below in §3.2 we need an estimate for ϕ_0 near the corner points of ∂D_s. Near these points, it suffices to use the expression for ϕ_0 in (3.6) that is valid for $r > r_b$,

$$\phi_0 \sim R_0 a_+ \nu_+^\epsilon (r_b/r)^{1/2} e^{-\nu_+^\epsilon \epsilon^{-1}(r-r_b)}\,. \tag{3.8}$$

To see this, we note that (3.6) satisfies exactly the no-flux boundary condition (3.4b) on the straight segment ∂D_s. To satisfy the no-flux boundary condition on ∂D_c, a boundary layer correction term localized near ∂D_c should be added to the expression in (3.6) that is valid for $r > r_b$. However, since the boundary layer is initiated near the corner regions of ∂D_s, the boundary layer correction term is asymptotically algebraically smaller for $\epsilon \ll 1$ than (3.8) in these regions, and hence can be neglected.

Next, we calculate the eigenpair associated with the nearly translation invariant degeneracy in the x-direction. This eigenfunction can be approximated by $\phi_1 \sim R_1 \partial_x U_b(r;\epsilon)$ where R_1 is a normalization constant. The corresponding eigenvalue is exponentially small. The function $\partial_x U_b(r;\epsilon)$ exactly satisfies (3.4a) with $\lambda = 0$ and it satisfies (3.4b) on ∂D_s. A boundary layer profile, localized near ∂D_c, should be added to this function to allow

it to satisfy the non-flux boundary condition on ∂D_c. However, as remarked above, the boundary layer profile has an asymptotically negligible effect on the eigenfunction near the corner regions where the boundary layer is initiated. Hence, we can use (3.2) for U_b to get the following estimate for $\phi_1 \sim R_1 \partial_x U_b$ near the corner regions:

$$\phi_1 \sim R_1 a_+ \nu_+^\epsilon \epsilon^{-1} (r_b/r)^{1/2} r^{-1} (x - x_0) e^{-\nu_+^\epsilon \epsilon^{-1}(r - r_b)} \,. \tag{3.9}$$

Applying Green's identity to ϕ_1 and $\partial_x U_b$, and using the facts that $\partial_n \phi_1 = 0$ on ∂D and $\partial_n [\partial_x U_b] = 0$ on ∂D_s, we obtain

$$\lambda_1 \left(\partial_x U_b, \phi_1 \right) = -\epsilon^2 \int_{\partial D_c} \phi_1 \partial_n [\partial_x U_b] \, ds \,. \tag{3.10}$$

Using (3.2), we calculate on ∂D_c that

$$\partial_n [\partial_x U_b] \sim -a_+ (\nu_+^\epsilon)^2 \epsilon^{-2} (r_b/r)^{1/2} r^{-1} (x - x_0) e^{-\nu_+^\epsilon \epsilon^{-1}(r - r_b)} \hat{\mathbf{r}} \cdot \hat{\mathbf{n}} \,. \tag{3.11}$$

Here $\hat{\mathbf{n}}$ is the outward unit normal vector to ∂D, $r = |\boldsymbol{x} - \boldsymbol{x}_0|$, and $\hat{\mathbf{r}} = (x - x_0, y)/r$ is a unit vector pointing from $(x_0, 0)$ to (x, y). The dominant contribution to the inner product on the left-hand side of (3.10) arises from the region near $r = r_b$. Using Laplace's method, we get for $\epsilon \ll 1$ that

$$\left(\partial_x U_b, \phi_1 \right) \sim \frac{\pi r_b \beta R_1}{2\epsilon} \,. \tag{3.12}$$

Since $\phi_1 \sim R_1 \partial_x U_b$, the normalization constant R_1 satisfies

$$R_1 \sim \left[2\epsilon / (\pi r_b \beta) \right]^{1/2} \,. \tag{3.13}$$

The dominant contribution as $\epsilon \to 0$ to the boundary integral on the right-hand side of (3.10) arises from the regions where r is the smallest. These regions are near the corner points. Substituting (3.9) and (3.11)–(3.13) into (3.10), we obtain an asymptotic estimate for λ_1

$$\lambda_1 \sim \frac{2 a_+^2 (\nu_+^\epsilon)^3}{\pi \beta} \int_{\partial D_c} r^{-1} \left(\frac{x - x_0}{r} \right)^2 e^{-2\nu_+^\epsilon \epsilon^{-1}(r - r_b)} \hat{\mathbf{r}} \cdot \hat{\mathbf{n}} \, ds \,. \tag{3.14}$$

To evaluate the integral in (3.14) asymptotically we use Laplace's method. The dominant contribution to this integral arises from $O(\epsilon)$ regions near the corner points $(x_L, 0)$ and $(x_R, 0)$. Near these points, we calculate that

$$\hat{\mathbf{r}} \cdot \hat{\mathbf{n}} \sim \begin{cases} c_L (x_L - x)^{\alpha_L} \,, & \text{as} \quad x \to x_L^- \,, \\ c_R (x - x_R)^{\alpha_R} \,, & \text{as} \quad x \to x_R^+ \,, \end{cases} \tag{3.15a}$$

$$r \sim \begin{cases} (x_0 - x_L) - (x - x_L) \,, & \text{as} \quad x \to x_L^- \,, \\ (x_R - x_0) + (x - x_R) \,, & \text{as} \quad x \to x_R^+ \,. \end{cases} \tag{3.15b}$$

Substituting (3.15) into (3.14), and applying Laplace's method, we get

$$\lambda_1 \sim \frac{2 a_+^2 (\nu_+^\epsilon)^3}{\pi \beta} \left\{ \frac{c_L I_L}{x_0 - x_L} e^{-2\nu_+^\epsilon \epsilon^{-1}(x_0 - x_L - r_b)} + \frac{c_R I_R}{x_R - x_0} e^{-2\nu_+^\epsilon \epsilon^{-1}(x_R - x_0 - r_b)} \right\} \,, \tag{3.16a}$$

where I_L and I_R are defined by

$$I_L \equiv \int_{-\infty}^{x_L} (x_L - x)^{\alpha_L} e^{-2\nu_+^\epsilon \epsilon^{-1}(x_L - x)}\, dx\,, \qquad I_R \equiv \int_{x_R}^{\infty} (x - x_R)^{\alpha_R} e^{-2\nu_+^\epsilon \epsilon^{-1}(x - x_R)}\, dx\,. \tag{3.16b}$$

The integrals in (3.16b) are evaluated explicitly by using

$$\int_0^\infty z^\alpha e^{-2z/\epsilon}\, dz = \left(\frac{\epsilon}{2}\right)^{\alpha+1} \Gamma(\alpha+1)\,, \tag{3.17}$$

where $\Gamma(z)$ is the Gamma function. In this way, we obtain the following main estimate for the exponentially small eigenvalue λ_1:

Proposition 3.1 (Eigenvalue): *Assume that the distance between $\boldsymbol{x}_0$ and ∂D_c is a minimum at either of the two corners $(x_L, 0)$ or $(x_R, 0)$. Then, for $\epsilon \to 0$, the second eigenvalue λ_1 of (3.4) has the asymptotic estimate*

$$\begin{aligned} \lambda_1 \;\sim\; & \frac{2a_+^2 (\nu_+^\epsilon)^3}{\pi\beta} \left\{ \frac{c_L}{x_0 - x_L} e^{-2\nu_+^\epsilon \epsilon^{-1}(x_0 - x_L - r_b)} \left(\frac{\epsilon}{2\nu_+^\epsilon}\right)^{\alpha_L+1} \Gamma(\alpha_L+1) \right. \\ & \left. + \frac{c_R}{x_R - x_0} e^{-2\nu_+^\epsilon \epsilon^{-1}(x_R - x_0 - r_b)} \left(\frac{\epsilon}{2\nu_+^\epsilon}\right)^{\alpha_R+1} \Gamma(\alpha_R+1) \right\}. \end{aligned} \tag{3.18}$$

Here a_+, ν_+^ϵ and β are defined in (A.5), (A.11), and (A.9b), respectively. The constants c_L, c_R, α_L and α_R are defined in (3.1) in terms of the local behavior of ∂D_c near the corner points.

3.2 The Slow Interface Motion

We now determine the motion of the semi-circular interface along ∂D_s. The center $\boldsymbol{x}_0 = (x_0(t), 0)$ of the semi-circle slowly slides along ∂D_s until either a steady-state solution is attained or the edge of the semi-circle first hits ∂D_c. The trajectory $x_0 = x_0(t)$, with $x_0(0) = x_0^0$, of the center of the circle is to be determined. It is assumed that the initial data is a canonical bubble solution $u(\mathbf{x}, 0) = U_b[|\mathbf{x} - \mathbf{x}_0^0|; \epsilon]$ with $\sigma = \sigma_b(\epsilon)$, and $\mathbf{x}_0^0 \equiv (x_0^0, 0)$. We set $u(\mathbf{x}, t) = U_b[|\mathbf{x} - \mathbf{x}_0|; \epsilon] + w(\mathbf{x}, t)$ and $\sigma(t) = \sigma_b + \mu(t)$. Linearizing (1.1) around U_b, and assuming that $w \ll U_b$ and $\mu \ll \sigma_b$ uniformly in time, we get

$$L_\epsilon w \equiv \epsilon^2 \Delta w + Q'(U_b) w = \partial_t U_b + \mu\,, \qquad \mathbf{x} \in D\,, \tag{3.19a}$$

$$\partial_n w = -\partial_n U_b, \qquad \mathbf{x} \in \partial D\,, \tag{3.19b}$$

$$\int_D w\, d\mathbf{x} = 0\,. \tag{3.19c}$$

Next, we expand $w = \sum_{j=0}^\infty c_j \phi_j / \lambda_j$, where ϕ_j, λ_j are the eigenpairs of (3.4). The coefficients c_j for $j \geq 0$, obtained by integration by parts, are given by

$$c_j = (\phi_j, \partial_t U_b) + \mu\,(\phi_j, 1) + \epsilon^2 \int_{\partial D_c} \phi_j \partial_n U_b\, ds\,. \tag{3.20}$$

In order to satisfy (3.19c), we require

$$\sum_{j=0}^{\infty} \frac{c_j}{\lambda_j} (\phi_j, 1) = 0 . \tag{3.21}$$

Since ϕ_0 has one sign and $\lambda_0 = O(\epsilon^2)$, (3.21) yields $c_0 = 0$ when $\epsilon \ll 1$. Next, since λ_1 is exponentially small we require that the limiting solvability condition $c_1 = 0$ be satisfied. Setting $c_0 = c_1 = 0$, we obtain two coupled equations for μ and x_0,

$$(\phi_0, \partial_t U_b) + \mu(\phi_0, 1) + \epsilon^2 \int_{\partial D_c} \phi_0 \partial_n U_b \, ds = 0 , \tag{3.22a}$$

$$(\phi_1, \partial_t U_b) + \mu(\phi_1, 1) + \epsilon^2 \int_{\partial D_c} \phi_1 \partial_n U_b \, ds = 0 . \tag{3.22b}$$

These two equations can be decoupled as follows. First, from (3.7)–(3.9) and (3.13), it can be seen that the two boundary integral terms in (3.22) have the same asymptotic order as $\epsilon \to 0$. Next, since ϕ_0 is even while ϕ_1 is odd in $x - x_0$, it follows from the exponential decay of both eigenfunctions for $r > r_b$ that $(\phi_0, 1)$ is exponentially larger than $(\phi_1, 1)$. Similarly, $(\phi_0, \partial_t U_b)$ is exponentially smaller than $(\phi_1, \partial_t U_b)$. Therefore, we can neglect $(\phi_0, \partial_t U_b)$ in (3.22a) and $\mu(\phi_1, 1)$ in (3.22b). This yields the uncoupled equations,

$$\mu(\phi_0, 1) \sim -\epsilon^2 \int_{\partial D_c} \phi_0 \partial_n U_b \, ds , \qquad (\phi_1, \partial_t U_b) \sim -\epsilon^2 \int_{\partial D_c} \phi_1 \partial_n U_b \, ds . \tag{3.23}$$

Next, we evaluate the terms in (3.23). Since ϕ_0, given in (3.6), is localized near $r = r_b$ we calculate that

$$(\phi_0, 1) \sim \epsilon \pi R_0 r_b (s_+ - s_-) . \tag{3.24}$$

The dominant contribution to the inner product $(\phi_1, \partial_t U_b)$ also arises from the region near $r = r_b$. Using $\phi_1 \sim R_1 \partial_x U_b$, we calculate

$$(\phi_1, \partial_t U_b) \sim -x_0'(t) R_1 \int_D [U_b']^2 \left(\frac{x - x_0}{r} \right)^2 d\mathbf{x} \sim -x_0'(t) \frac{R_1 r_b}{\epsilon} \int_0^{\pi} \int_{-\infty}^{\infty} [u_0'(\rho)]^2 \cos^2\theta \, d\rho \, d\theta . \tag{3.25a}$$

Thus,

$$(\phi_1, \partial_t U_b) \sim -x_0'(t) \left(\frac{R_1 r_b \pi \beta}{2\epsilon} \right) , \tag{3.25b}$$

where β is defined in (A.9b). The dominant contribution to the boundary integral terms in (3.23) arises from the corner regions where r is minimized. Using (3.8) for ϕ_0, (3.9) for ϕ_1, and (3.2) to calculate $\partial_n U_b$, (3.23) becomes

$$\mu(t) \sim -\frac{a_+^2 (\nu_+^\epsilon)^2}{\pi (s_+ - s_-)} \int_{\partial D_c} r^{-1} e^{-2\nu_+^\epsilon \epsilon^{-1}(r - r_b)} \, \hat{\mathbf{r}} \cdot \hat{\mathbf{n}} \, ds , \tag{3.26a}$$

$$x_0'(t) \sim \frac{2\epsilon a_+^2 (\nu_+^\epsilon)^2}{\pi \beta} \int_{\partial D_c} r^{-1} \left(\frac{x - x_0}{r} \right) e^{-2\nu_+^\epsilon \epsilon^{-1}(r - r_b)} \, \hat{\mathbf{r}} \cdot \hat{\mathbf{n}} \, ds . \tag{3.26b}$$

Evaluating the integrals by Laplace's method, and using the local behavior (3.15) near the corners, we get

$$\mu(t) \sim -\frac{a_+^2(\nu_+^\epsilon)^2}{\pi(s_+ - s_-)}\left\{\frac{c_L I_L}{x_0 - x_L}e^{-2\nu_+^\epsilon \epsilon^{-1}(x_0 - x_L - r_b)} + \frac{c_R I_R}{x_R - x_0}e^{-2\nu_+^\epsilon \epsilon^{-1}(x_R - x_0 - r_b)}\right\}, \tag{3.27a}$$

$$x_0'(t) \sim \frac{2\epsilon a_+^2(\nu_+^\epsilon)^2}{\pi\beta}\left\{\frac{c_R I_R}{x_R - x_0}e^{-2\nu_+^\epsilon \epsilon^{-1}(x_R - x_0 - r_b)} - \frac{c_L I_L}{x_0 - x_L}e^{-2\nu_+^\epsilon \epsilon^{-1}(x_0 - x_L - r_b)}\right\}, \tag{3.27b}$$

where I_L and I_R are defined in (3.16b). Finally, (3.17) is used in (3.27) to obtain the following slow motion result:

Proposition 3.2 (Metastability): *Assume that the distance between $\boldsymbol{x}_0$ and ∂D_c is a minimum at either of the two corners $(x_L, 0)$ or $(x_R, 0)$. Then, for $\epsilon \to 0$, the location of the center of the semi-circular interface along ∂D_s satisfies the asymptotic differential equation*

$$\begin{aligned} x_0'(t) \;\sim\; & \frac{2\epsilon a_+^2(\nu_+^\epsilon)^2}{\pi\beta}\left\{\frac{c_R}{x_R - x_0}e^{-2\nu_+^\epsilon \epsilon^{-1}(x_R - x_0 - r_b)}\left(\frac{\epsilon}{2\nu_+^\epsilon}\right)^{\alpha_R+1}\Gamma(\alpha_R+1)\right. \\ & \left. - \frac{c_L}{x_0 - x_L}e^{-2\nu_+^\epsilon \epsilon^{-1}(x_0 - x_L - r_b)}\left(\frac{\epsilon}{2\nu_+^\epsilon}\right)^{\alpha_L+1}\Gamma(\alpha_L+1)\right\}. \end{aligned} \tag{3.28a}$$

The Lagrange multiplier parameter is $\sigma = \sigma_b + \mu$, where σ_b is given in (3.3), and where μ satisfies

$$\begin{aligned} \mu(t) \;\sim\; & -\frac{a_+^2(\nu_+^\epsilon)^2}{\pi(s_+ - s_-)}\left\{\frac{c_L}{x_0 - x_L}e^{-2\nu_+^\epsilon \epsilon^{-1}(x_0 - x_L - r_b)}\left(\frac{\epsilon}{2\nu_+^\epsilon}\right)^{\alpha_L+1}\Gamma(\alpha_L+1)\right. \\ & \left. + \frac{c_R}{x_R - x_0}e^{-2\nu_+^\epsilon \epsilon^{-1}(x_R - x_0 - r_b)}\left(\frac{\epsilon}{2\nu_+^\epsilon}\right)^{\alpha_R+1}\Gamma(\alpha_R+1)\right\}. \end{aligned} \tag{3.28b}$$

Referring to (3.28a), we see that the motion of the center of the semi-circular interface along ∂D_s is determined by the local boundary behavior (3.1) near the corner points and by the distance from the interface to these points. The interface will move according to (3.28a), without change of shape, until a stable steady-state is reached or until the interface first touches $(x_L, 0)$ or $(x_R, 0)$. Once the interface has reached ∂D_c, it will subsequently evolve according to (1.3). Differential equations similar to (3.28a) have been derived in [5], [14] and [17] for the motion of straight-line interfaces for the Allen-Cahn equation that are trapped in a constant cross-sectional neck region of a dumbell-shaped domain.

3.3 Steady States and Explicit Dynamics

When c_L and c_R have the same signs, (3.28a) has an equilibrium solution x_0^e that satisfies

$$\left(\frac{x_0^e - x_L}{x_R - x_0^e}\right)e^{4\nu_+^\epsilon \epsilon^{-1} x_0^e} = \frac{c_L\Gamma(\alpha_L+1)}{c_R\Gamma(\alpha_R+1)}\left(\frac{\epsilon}{2\nu_+^\epsilon}\right)^{\alpha_L - \alpha_R}e^{2\nu_+^\epsilon \epsilon^{-1}(x_R + x_L)}. \tag{3.29}$$

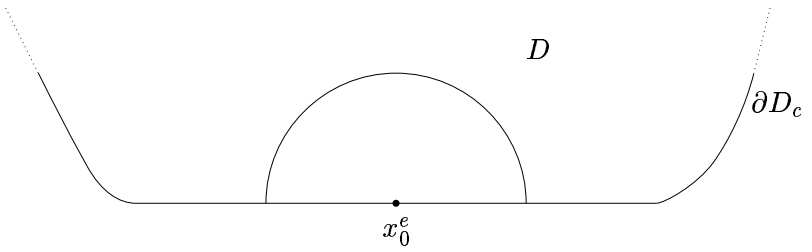

Figure 9: Plot of part of a domain boundary, ∂D, upon which the center of the semi-circular interface is at an unstable steady state. Note that c_L, $c_R > 0$ for this domain.

Since the left side of (3.29) increases monotonically from 0 to ∞ as x_0^e ranges from x_L to x_R, a unique steady-state solution exists on the interval $[x_L, x_R]$ whenever c_L and c_R have the same sign. In this case, the solution to (3.29) is given asymptotically for $\epsilon \ll 1$ by

$$x_0^e \sim \frac{x_L + x_R}{2} + \frac{\epsilon}{4\nu_+^\epsilon} \log\left[\frac{c_L \Gamma(\alpha_L + 1)}{c_R \Gamma(\alpha_R + 1)} \left(\frac{\epsilon}{2\nu_+^\epsilon}\right)^{\alpha_L - \alpha_R}\right] + \cdots . \tag{3.30}$$

Thus, x_0^e is located at an $O(\epsilon)$ distance from the midpoint of ∂D_s. This steady-state solution is stable when $c_L < 0$ and $c_R < 0$, and is unstable when $c_L > 0$ and $c_R > 0$. In particular, this implies that if D is convex near $(x_L, 0)$ and $(x_R, 0)$, then there is no stable equilibrium location on ∂D_s.

We now illustrate the dynamics when $Q(u) = 2(u - u^3)$, for which $s_\pm = \pm 1$. Using (A.5), (A.9b), and (A.11), the constants $a_\pm$, β and $\nu_\pm^\epsilon$, are found to be

$$a_\pm = 2\,, \qquad \beta = 4/3\,, \qquad \nu_\pm^\epsilon = 2\left(1 - \frac{\epsilon}{4r_b}\right) . \tag{3.31}$$

We consider the case when $\alpha_L = \alpha_R = \alpha > 0$. Then, (3.28a) reduces to

$$x_0' \sim \frac{6\epsilon^{\alpha+2}\Gamma(\alpha+1)}{4^\alpha \pi}\left[\frac{c_R}{x_R - x_0} e^{-2\nu_+^\epsilon \epsilon^{-1}(x_R - x_0 - r_b)} - \frac{c_L}{x_0 - x_L} e^{-2\nu_+^\epsilon \epsilon^{-1}(x_0 - x_L - r_b)}\right] . \tag{3.32}$$

When $c_L c_R > 0$, the equilibrium location satisfies

$$x_0^e \sim \frac{x_L + x_R}{2} + \frac{\epsilon}{8} \log\left(\frac{c_L}{c_R}\right) . \tag{3.33}$$

With the initial condition $x_0^0(0)$, the following qualitative features of the motion can be deduced from (3.32) and (3.33). When $c_L > 0$ and $c_R > 0$, $x_0(t)$ will move monotonically towards x_L if $x_0^0 < x_0^e$, or monotonically towards x_R if $x_0^0 > x_0^e$ (see Fig. 9). When $c_L < 0$ and $c_R < 0$, $x_0(t)$ will approach the stable steady state at x_0^e (see Fig. 10). If $c_L < 0$ and $c_R > 0$, then $x_0(t)$ will move towards x_R (see Fig. 11). Similarly, $x_0(t)$ will move towards x_L if $c_L > 0$ and $c_R < 0$. In each case the motion is directed towards a region where the length of the perimeter of the interface can be decreased while still enclosing the same area.

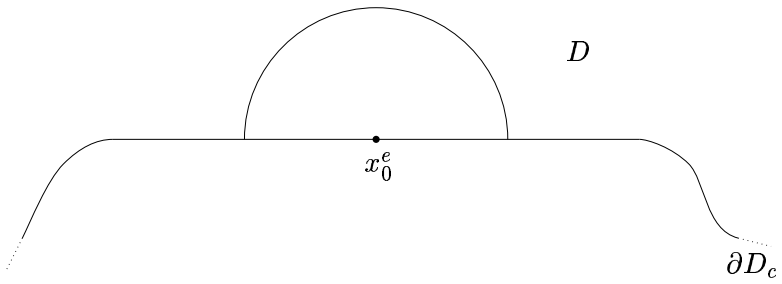

Figure 10: Plot of part of a domain boundary, ∂D, upon which the center of the semi-circular interface is at a stable steady state. Note that c_L, $c_R < 0$ for this domain.

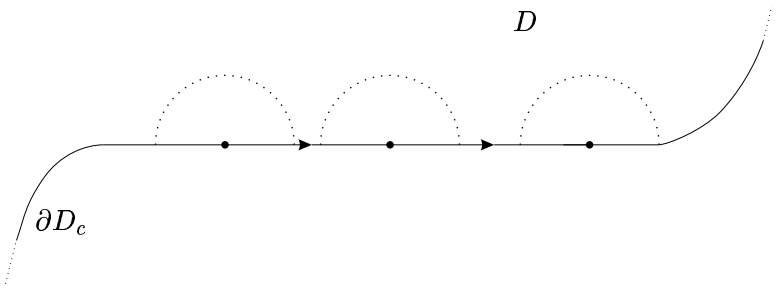

Figure 11: Plot of part of a domain boundary, ∂D, upon which the center of the semi-circular interface moves toward the right. Note that $c_L < 0$ and $c_R > 0$ for this domain.

4 Conclusions

We have studied the motion of interfaces for (1.1) that are attached orthogonally to the boundary of a two-dimensional domain. A numerical computation of the area-preserving mean curvature flow using a front-tracking method has shown that the asymptotic differential equation (1.5) of [2], derived in the limit $\epsilon \ll 1$ and for small drop radius δ, is also rather accurate even for moderately small values of δ. In addition, we have studied the exponentially slow motion of a semi-circular interface attached to a flat portion of the boundary by deriving a differential equation for the motion of the center of the interface.

It is interesting to note that other nonlocal reaction-diffusion equations can have similar qualitative dynamics. In particular, results similar to those obtained here have recently been derived for a nonlocal reaction-diffusion equation arising from an asymptotic limit of the Gierer-Meinhardt activator-inhibitor system. This system admits localized solutions in the form of spikes and the qualitative spike motion is quite similar to that described in Fig. 1b–1f. The metastable motion of interior spikes has been studied in [12] and [8]. Results for the equilibria of boundary spikes are given in [10]. The motion of boundary spikes, which is similar to (1.5), is studied in [13].

Acknowledgements

M. J. W. is grateful for the gracious hospitality of Hillary and John Ockendon of the Oxford Center for Industrial and Applied Mathematics at Oxford University where this paper was written.

A The Canonical Bubble Solution

Here we calculate a radially symmetric solution $u = U_b(r;\epsilon)$, $\sigma = \sigma_b(\epsilon)$ to the equilibrium problem for (1.1). This solution will represent a semi-circular interfacial solution of radius $r = r_b$, where $r = |\boldsymbol{x} - \boldsymbol{x}_0|$ and $\boldsymbol{x}_0 = (x_0, 0)$. The functions $U_b(r;\epsilon)$ and $\sigma_b(\epsilon)$, satisfy

$$\epsilon^2\left(U_b'' + \frac{1}{r}U_b'\right) + Q(U_b) = \sigma_b\,, \qquad 0 < r < \infty\,; \qquad U_b' > 0\,, \tag{A.1a}$$

$$U_b(r_b;\epsilon) = 0\,; \qquad U_b(r;\epsilon) \to S_\pm(\epsilon)\,, \qquad \text{as} \qquad \epsilon^{-1}(r - r_b) \to \pm\infty\,. \tag{A.1b}$$

Here $S_\pm(\epsilon)$ are defined as the roots of

$$Q\left[S_\pm(\epsilon)\right] = \sigma_b(\epsilon)\,, \tag{A.2}$$

for which $S_\pm(\epsilon) \to s_\pm$ and $\sigma_b(\epsilon) \to 0$ as $\epsilon \to 0$.

The method of matched asymptotic expansions as described in [16] is used to construct the solution. In the inner region near the interface, we let $\rho \equiv \epsilon^{-1}(r - r_b) = O(1)$ and define $u_b(\rho;\epsilon) = U_b(r_b + \epsilon\rho;\epsilon)$. From (A.1) we obtain

$$u_b'' + \frac{\epsilon}{r_b + \epsilon\rho}u_b' + Q(u_b) = \sigma_b\,, \qquad -\infty < \rho < \infty\,; \qquad u_b' > 0\,, \tag{A.3a}$$

$$u_b(0;\epsilon) = 0\,; \qquad u_b(\rho;\epsilon) \to S_\pm(\epsilon) \quad \text{as } \rho \to \pm\infty\,. \tag{A.3b}$$

Then, to leading order as $\epsilon \to 0$, we have that $S_\pm(\epsilon) \to s_\pm$, $\sigma_b(\epsilon) \to 0$, and $u_b(\rho;\epsilon) \to u_0(\rho)$, where $u_0(\rho)$ satisfies the one-dimensional planar interface problem

$$u_0'' + Q(u_0) = 0\,, \qquad -\infty < \rho < \infty\,; \qquad u_0' > 0\,, \qquad u_0(0;\epsilon) = 0\,, \tag{A.4a}$$

$$u_0(\rho) \sim s_+ - a_+ e^{-\nu_+\rho} \quad \rho \to \infty\,; \qquad u_0(\rho) \sim s_- + a_- e^{\nu_-\rho} \quad \rho \to -\infty\,. \tag{A.4b}$$

Here the positive constants $\nu_\pm$ and $a_\pm$ are defined by

$$\nu_\pm = \left[-Q'(s_\pm)\right]^{1/2}\,, \qquad \log a_\pm = \log(\pm s_\pm) + \int_0^{s_\pm}\left(\frac{\pm\nu_\pm}{[2V(\eta)]^{1/2}} + \frac{1}{\eta - s_\pm}\right)d\eta\,, \tag{A.5}$$

where $V(u) \equiv -\int_{s_-}^{u} Q(\eta)\,d\eta$.

We expand the solution to (A.3) as

$$u_b(\rho;\epsilon) \sim \sum_{j=0}^{\infty}\epsilon^j u_j(\rho)\,, \qquad \sigma_b(\epsilon) \sim \sum_{j=1}^{\infty}\epsilon^j\sigma_j\,, \qquad S_\pm(\epsilon) \sim s_\pm + \sum_{j=1}^{\infty}\epsilon^j u_j(\pm\infty)\,. \tag{A.6}$$

Substituting (A.6) into (A.3), we obtain for some functions G_j and $g_{j\pm}$, that u_j for $j \geq 1$ satisfies

$$Lu_j \equiv u_j'' + Q'(u_0)u_j = \sigma_j + G_j(u_0, \ldots, u_{j-1}), \qquad -\infty < \rho < \infty; \tag{A.7a}$$

$$u_j(\rho) \to -\sigma_j \nu_\pm^{-2} + g_{j\pm}(\sigma_1, \ldots, \sigma_{j-1}), \quad \text{as } \rho \to \pm\infty; \qquad u_j(0) = 0. \tag{A.7b}$$

¿From (A.4) we see that $Lu_0' = 0$ and $u_0'(\pm\infty) = 0$. Thus, the right side of (A.7a) produces a solvability condition that determines σ_j as

$$\sigma_j = \frac{-1}{(s_+ - s_-)} \int_{-\infty}^{\infty} u_0' \, G_j(u_0, \ldots, u_{j-1}) \, d\rho, \qquad \text{for} \qquad j \geq 1. \tag{A.8}$$

Equations (A.2), (A.6), and (A.8) determine the asymptotic expansions for $u_b(\rho;\epsilon)$, $\sigma_b(\epsilon)$, and $S_\pm(\epsilon)$. These conditions give

$$S_\pm(\epsilon) = s_\pm - \frac{\epsilon\sigma_1}{\nu_\pm^2} + O(\epsilon^2), \qquad \sigma_1 = \frac{\beta}{(s_+ - s_-)r_b}, \tag{A.9a}$$

where

$$\beta \equiv \int_{-\infty}^{\infty} \left[u_0'(\rho)\right]^2 d\rho = \sqrt{2} \int_{s_-}^{s_+} [V(u)]^{1/2} \, du. \tag{A.9b}$$

In the outer region for $r > r_b$ we write $U_b(r;\epsilon) = S_+(\epsilon) + u_+(r;\epsilon)$, where $u_+ \ll S_+$. Similarly, in the region where $r < r_b$ we let $U_b(r;\epsilon) = S_-(\epsilon) + u_-(r;\epsilon)$, where $u_- \ll S_-$. We linearize (A.1a) about $S_\pm$ to obtain that

$$u_+'' + r^{-1}u_+' - (\epsilon^{-1}\nu_+^\epsilon)^2 u_+ = 0, \qquad r > r_b, \tag{A.10a}$$

$$u_-'' + r^{-1}u_-' - (\epsilon^{-1}\nu_-^\epsilon)^2 u_- = 0, \qquad r < r_b. \tag{A.10b}$$

Here $\nu_\pm^\epsilon = (-Q'[S_\pm(\epsilon)])^{1/2}$. Then, using (A.9a) for $S_\pm$, we can calculate $\nu_\pm^\epsilon$ for $\epsilon \ll 1$ to get

$$\nu_\pm^\epsilon = \nu_\pm \left[1 + \frac{\epsilon\sigma_1}{2\nu_\pm^4} Q''(s_\pm) + O(\epsilon^2)\right]. \tag{A.11}$$

Equations (A.10a), (A.10b) can be solved exactly in terms of the modified Bessel functions K_m and I_m. Using the large argument expansion of these functions and matching to the far-field behavior of the inner solution, we obtain (3.2).

B The Principal Eigenpair

This appendix summarizes the calculations of [16] to asymptotically estimate the principal eigenpair ϕ_0, λ_0 of (3.4). The principal eigenfunction is locally radially symmetric near $r = r_b$.

In the internal layer region we set $\rho = \epsilon^{-1}(r - r_b)$ and $\Phi_0(\rho;\epsilon) = \phi_0(r_b + \epsilon\rho)$. We then expand

$$\Phi_0(\rho;\epsilon) \sim \sum_{j=0}^{\infty} \epsilon^j \Phi_{0j}(\rho), \qquad \lambda_0(\epsilon) \sim \sum_{j=0}^{\infty} \epsilon^j \lambda_{0j}. \tag{B.1}$$

Substituting $U_b(r;\epsilon) \sim \sum_{j=0}^{\infty} \epsilon^j u_j(\rho)$ and (B.1) into (3.4a), we get the hierarchy

$$L\Phi_{00} = \lambda_{00}\Phi_{00}\,, \tag{B.2a}$$

$$L\Phi_{01} = -u_1\Phi_{00}Q_0'' - r_b^{-1}\Phi_{00}' + \lambda_{01}\Phi_{00} + +\lambda_{00}\Phi_{01}\,, \tag{B.2b}$$

$$L\Phi_{02} = -r_b^{-1}\Phi_{01}' + \rho r_b^{-2}\Phi_{00}' - u_1\Phi_{01}Q_0'' - u_2\Phi_{00}Q_0'' - \frac{1}{2}u_1^2\Phi_{00}Q_0'' + \lambda_{00}\Phi_{02} + \lambda_{01}\Phi_{01} + \lambda_{02}\Phi_{00}\,. \tag{B.2c}$$

Here $Q_0'' \equiv Q''(u_0)$, and Lv is defined in (A.7a). The required far-field behavior is that $\Phi_{0j}(\rho) \to 0$ as $\rho \to \pm\infty$. Since $Lu_0' = 0$ and $u_0'(\pm\infty) = 0$, we have the solvability condition that $L\Phi_{0j}$ for $j = 0, 1, 2$ is orthogonal to u_0'. This condition is used to determine Φ_{0j} and λ_{0j}. The results are

$$\Phi_0(\rho;\epsilon) = R_0\left[u_0'(\rho) + O(\epsilon)\right]\,; \qquad \lambda_0 = \epsilon^2/r_b + O(\epsilon^3)\,, \tag{B.3}$$

where R_0 is a normalization constant and u_0 satisfies (A.4).

In the outer regions where $U_b \sim S_{\pm}(\epsilon)$, we let $\phi_0 \sim R_0\phi_+(r;\epsilon)$ and $\phi_0 \sim R_0\phi_-(r;\epsilon)$ for $r > r_b$ and $r < r_b$, respectively. Then (3.4a) becomes

$$\phi_+'' + r^{-1}\phi_+' - \left(\epsilon^{-1}\tilde{\nu}_+^{\epsilon}\right)^2\phi_+ = 0\,, \qquad r > r_b\,, \tag{B.4a}$$

$$\phi_-'' + r^{-1}\phi_-' - \left(\epsilon^{-1}\tilde{\nu}_-^{\epsilon}\right)^2\phi_- = 0\,, \qquad r < r_b\,. \tag{B.4b}$$

Here we have defined $\tilde{\nu}_{\pm}^{\epsilon} \equiv \nu_{\pm}^{\epsilon}[1 + \lambda_0/(\nu_{\pm}^{\epsilon})^2]^{1/2}$. These equations can be solved in terms of modified Bessel functions and the solutions matched to (B.3), to produce (3.6). The normalization constant R_0 is found from the condition $(\phi_0, \phi_0) = 1$. Evaluating this inner product asymptotically we get $R_0 \sim (\epsilon\pi r_b\beta)^{-1/2}$, where β was defined in (A.9b).

References

[1] N. Alikakos, L. Bronsard, G. Fusco, *Slow Motion in the Gradient Theory of Phase Transitions via Energy and Spectrum*, Calc. Var. Part. Diff. Eq. **6**, No. 1, (1998), pp. 39–66.

[2] N. Alikakos, X. Chen, G. Fusco, *Motion of a Drop by Surface Tension Along the Boundary*, to appear, J. of Geometric Analysis, (1999).

[3] N. Alikakos, G. Fusco, *Slow Dynamics for the Cahn-Hilliard Equation in Higher Spatial Dimensions, Part 2: the Motion of Bubbles*, Arch. Rat. Mech. Anal. **141**, (1998), pp. 1–61.

[4] N. Alikakos, G. Fusco, *Some Aspects of the Dynamics of the Cahn-Hilliard Equation*, Resenhas **1**, No. 4, (1994), pp. 517–530.

[5] N. Alikakos, G. Fusco, M. Kowalczyk, *Finite Dimensional Dynamics and Interfaces Intersecting the Boundary: Equilibria and Quasi-Invariant Manifold*, Indiana Univ. Math. J. **45**, No. 4, (1996), pp. 1119–1155.

[6] L. Bronsard, B. Wetton, *A Numerical Method for Tracking Curve Networks Moving with Curvature Motion*, J. Comp. Phys. **120**, No. 1, (1995), pp. 66–87.

[7] X. Chen, M. Kowalczyk, *Existence of Equilibria for the Cahn-Hilliard Equation via Local Minimizers of the Perimeter*, Comm. Part. Diff. Equat. **21**, No. 7-8, (1996), pp. 1207–1233.

[8] X. Chen, M. Kowalczyk, *Slow Dynamics of Interior Spikes in the Shadow Gierer-Meinhardt System*, Center for Nonlinear Analysis report No. 99-CNA-002 Carnegie-Mellon University, (1999), preprint.

[9] M. Gage, *On an Area-Preserving Evolution For Plane Curves*, Contemp. Math. **51**, (1986), pp. 51–62.

[10] C. Gui, *Multi-peaked Solutions to a Semilinear Neumann Problem*, Duke Math. J., **84**, No.3, (1996), pp. 739-769.

[11] C. Hsiung, *A First Course in Differential Geometry*, Wiley Interscience Series in Pure and Applied Mathematics, Wiley, New York, (1981).

[12] D. Iron, M. J. Ward, *A Metastable Spike Solution for a NonLocal Reaction-Diffusion Model*, SIAM J. Appl. Math., (1999), to appear.

[13] D. Iron, M. J. Ward, *The Dynamics of Boundary Spikes for a Nonlocal Reaction-Diffusion Model*, submitted, Europ. J. Applied Math, (1999).

[14] M. Kowalczyk, *Exponentially Slow Dynamics and Interfaces Intersecting the Boundary*, J. Diff. Eq. **138**, No. 1, (1997), pp. 55-85.

[15] J. Rubinstein, P. Sternberg, *Nonlocal Reaction-Diffusion Equations and Nucleation*, IMA J. Appl. Math. **48**, (1992), pp. 249–264.

[16] M. J. Ward, *Metastable Bubble Solutions for the Allen-Cahn Equation with Mass Conservation*, SIAM J. Appl. Math. **56**, No. 5, (1996), pp. 1247–1279.

[17] M. J. Ward, D. Stafford, *Metastable Dynamics and Spatially Inhomogeneous Equilibria in Dumbell-Shaped Domains*, to appear, Studies in Appl. Math, (1999).